Check for updates

AGU ADVANCING EARTH AND SPACE SCIENCES

Earth and Space Science

RESEARCH ARTICLE
10.1029/2025EA004305

Direct Observations of Surface Fluxes and Air-Sea Exchange Coefficients in Low Winds Using a Small Uncrewed Aircraft System

Christopher J. Deloach[1], Joshua B. Wadler[1], Guo Lin[2,3], Joseph J. Cione[2], Jun A. Zhang[2,3], Jack S. Elston[4], and Maciej Z. Stachura[4]

[1]Embry-Riddle Aeronautical University/Department of Applied Aviation Sciences, Daytona Beach, FL, USA, [2]NOAA Atlantic Oceanographic and Meteorological Laboratory/Hurricane Research Division, Miami, FL, USA, [3]University of Miami Cooperative Institute for Marine and Atmospheric Studies, Miami, FL, USA, [4]Black Swift Technologies, Boulder, CO, USA

Key Points:

- First ever small Uncrewed Aircraft System (UAS) flight that measured air-sea interactions at ∼10 m above sea level
- The small UAS measured air-sea fluxes directly and using bulk aerodynamic formula
- Data from the mission is used to find boundary layer exchange coefficients in low winds

Correspondence to:
C. J. Deloach,
deloacc1@my.erau.edu

Citation:
Deloach, C. J., Wadler, J. B., Lin, G., Cione, J. J., Zhang, J. A., Elston, J. S., & Stachura, M. Z. (2025). Direct observations of surface fluxes and air-sea exchange coefficients in low winds using a small uncrewed aircraft system. *Earth and Space Science*, *12*, e2025EA004305. https://doi.org/10.1029/2025EA004305

Received 5 MAR 2025
Accepted 24 JUN 2025

Author Contributions:
Conceptualization: Joshua B. Wadler, Guo Lin
Data curation: Joshua B. Wadler, Joseph J. Cione, Jun A. Zhang, Maciej Z. Stachura
Formal analysis: Christopher J. Deloach, Joshua B. Wadler, Guo Lin, Maciej Z. Stachura
Funding acquisition: Joshua B. Wadler, Joseph J. Cione, Jun A. Zhang
Investigation: Christopher J. Deloach, Joshua B. Wadler
Methodology: Joshua B. Wadler
Project administration: Joseph J. Cione
Resources: Jack S. Elston, Maciej Z. Stachura
Software: Jack S. Elston, Maciej Z. Stachura
Supervision: Christopher J. Deloach, Jun A. Zhang
Validation: Christopher J. Deloach, Joshua B. Wadler, Guo Lin, Joseph J. Cione

© 2025. The Author(s).
This is an open access article under the terms of the Creative Commons Attribution License, which permits use, distribution and reproduction in any medium, provided the original work is properly cited.

Abstract In the marine boundary layer, the exchange of momentum, heat, and moisture occurs between the atmosphere and ocean. Since it is too dangerous for a crewed aircraft to fly close to the ocean surface to directly obtain these measurements, a sUAS (small Uncrewed Aircraft System) is one of the only viable options. On 24 March 2023 a Black Swift Technologies S0 sUAS was deployed from the NOAA P-3 on a calm clear day off the west coast of Florida. For 23 min at the end of the mission, the sUAS flew 8 straight line legs with an average length of 2.15 km, at roughly 10 m above the ocean surface, with wind speeds between 3.0 and 4.5 m s^{-1}. For the first time over the open ocean using a sUAS, the 4-Hz wind and thermodynamic data was used to calculate surface momentum flux, sensible heat flux, and latent flux using both direct covariance methods and the bulk aerodynamic formulas. Since all the flux quantities can be found using both direct and indirect methods, we are able to calculate the exchange coefficients of momentum flux (C_D), latent heat flux (C_E), and sensible heat flux (C_H) with results that are generally in good agreement with previous studies over the same wind speed range. This study demonstrates the ability of sUAS to measure air-sea interactions. Future intention is to use sUAS to obtain similar measurements in high wind events such as hurricanes which could better help understand hurricane intensification and improve model physics.

Plain Language Summary To understand the exchange of momentum, heat, and moisture between the ocean and atmosphere, continuous measurements need to be taken at 10 m altitude which has historically been challenging due to safety constraints of crewed aircraft. This study demonstrates the first time a sUAS (small Uncrewed Aircraft System) collected measurements near that altitude over the ocean. Previous studies using crewed aircraft to study the marine boundary layer did not have the ability to fly at low levels of the atmosphere and other studies had to utilize different instruments to measure this regime. This study shows the significance of using sUAS for data collection in the lower atmosphere with the goal of deploying into hurricanes to improve understanding of storm structure and model forecasting of storms.

1. Introduction

Measurements of surface fluxes of momentum, heat, and moisture in high wind conditions such as tropical cyclones (TCs) are incredibly difficult to obtain due to the dangers of flying crewed aircraft close to the sea surface. Many studies have attempted to estimate the exchange coefficient of momentum transfer (i.e., drag coefficient, C_D) at high winds (Anderson, 1993; Andreas et al., 2012; Black et al., 2007; Businger, 1966, 1971; Donelan et al., 1997, 2004; Drennan et al., 1999; Dyer, 1974; Emanuel, 1986, 1995; Foreman & Emeis, 2010; French et al., 2007; Haus et al., 2010; Jarosz et al., 2007; Kitaigorodskii & Volkov, 1965; Large & Pond, 1981; Potter et al., 2015; Powell et al., 2003; Vickers et al., 2013). In general, it is currently understood that C_D increases roughly linearly between 4 m s^{-1} and ∼30 m s^{-1} with variations due to wave age and swell (e.g., Donelan et al., 1997; Drennan et al., 1999, 2003; Kitaigorodskii & Volkov, 1965; Volkov, 1970). Above ∼30 m s^{-1}, C_D levels off and potentially decreases with increasing wind speed, likely due to the aerodynamic influences of the waves (e.g., Donelan et al., 2004; Powell et al., 2003). There has also been studies highlighting the variability of C_D at low wind (e.g., ≲5 m s^{-1}) conditions (e.g., Andreas et al., 2012; Foreman & Emeis, 2010; Oost et al., 2000; Vickers et al., 2013), which is the focus of this manuscript. In this low wind speed regime, the behavior of C_D shows substantial variability where the calculated value depends on the choice of processing technique. For

23335084, 2025, 8, Downloaded from https://agupubs.onlinelibrary.wiley.com/doi/10.1029/2025EA004305 by Battelle Memorial Institute, Wiley Online Library on [02/09/2025]. See the Terms and Conditions (https://onlinelibrary.wiley.com/terms-and-conditions) on Wiley Online Library for rules of use; OA articles are governed by the applicable Creative Commons License

Visualization: Christopher J. Deloach, Joshua B. Wadler
Writing – original draft: Christopher J. Deloach, Joshua B. Wadler
Writing – review & editing: Christopher J. Deloach, Joshua B. Wadler, Guo Lin, Joseph J. Cione, Jun A. Zhang, Jack S. Elston

example, Vickers et al. (2013) showed derived C_D values ranging two orders of magnitude at 5 m s^{-1}. To date, no study has calculated C_D from direct aircraft measurements at 10 m height above the ocean surface. While the ultimate goal is to use small uncrewed aerial systems (sUASs) to estimate C_D in TCs, a goal of this manuscript is to demonstrate the ability to perform this calculation in measurements from low wind conditions.

The exchange coefficients for sensible heat transfer (C_H) and latent heat transfer (C_E) are generally less studied than C_D. Previous studies analyzing thermodynamic fluxes using direct eddy covariances (e.g., DeCosmo et al., 1996; Drennan et al., 2007; Zhang et al., 2008) generally show no trend with respect to wind speed when the winds are less than 30 m s^{-1}. While there are limitations in using a wave tank to estimate the exchange coefficients, due to the restrictions for wave age, wave height, spray, and fetch, the lack of trends in C_H and C_E were also seen by calculating energy budgets laboratory experiments by Haus et al. (2010) and Jeong et al. (2012).

The accurate representation of transfer coefficients is essential as numerical weather prediction models use them to estimate the turbulent exchange of momentum, heat, and moisture, which is closely tied to predicting TC intensity. Additionally, the ratio between the transfer coefficient of enthalpy (C_k) and C_D is a crucial factor in determining the maximum TC intensity (i.e., Emanuel, 1986, 1995). To achieve realistic intensity for a TC, the simulated ratio of C_K/C_D typically lies between 0.75 and 1.5 (Emanuel, 1995). However, with the data collected during six flights into hurricanes Fabian and Isabel (which were either Category 4 or 5 on the Saffir-Simpson scale), the average ratio C_K/C_D was 0.63 (Zhang et al., 2008), which was much lower than previously suggested for hurricane development and intensity in Emanuel (1995). To date, the factors that contribute to C_K/C_D still have relatively high uncertainty.

Due to the need to estimate these exchange coefficients, alternative methods besides the direct covariance method have been used. For example, Bell et al. (2012) used azimuthally averaged energy and angular momentum budgets to estimate the surface fluxes. Additionally, Richter et al. (2016) used dropwindsondes (often called dropsondes; Aberson et al., 2023; Hock & Franklin, 1999) to compute the exchange coefficients using the flux profile method. Both methods produced exchange coefficients with similar or higher amounts of uncertainty as previous studies using the direct eddy covariance method, though they had more data available at higher wind speeds.

More recent field campaigns to measure surface exchange coefficients in TCs such as the Coupled Boundary Layer Air-Sea Transfer (CBLAST) resulted in direct eddy covariance sensible and latent heat flux measurements in Hurricanes Fabian and Isabel in 2003 (Black et al., 2007; French et al., 2007; Zhang et al., 2008). These measurements were made from the NOAA WP-3D (P-3) aircraft in the non-precipitating moat regions between rain bands and in wind speeds up to 30 m s^{-1}. The data from CBLAST were recorded at roughly 60 m above the surface of the ocean with each path length being 30 km. For this experiment, the P-3 was outfitted with a 9-hole Best Aircraft Turbulence (BAT) probe which is a multi-hole pressure probe (MHPP) designed to provide direct measurements of three differential pressures which can be used to calculate three dimensional winds at a high (>50 Hz) frequency (French et al., 2007). Due to the dangers of flying close to the sea surface in the hurricane, measurements like that obtained in CBLAST are no longer possible on the NOAA P-3 aircraft since lower-level flights are disallowed for crewed aircrafts.

In recent years, sUASs have been developed to be air-deployed by the P-3 into TCs (Cione et al., 2016, 2020). The air-deployed sUAS currently being developed range in weight from 3 pounds to 27 pounds and are deployed from the A-sized sonobuoy chute typically used for releasing airborne expendable bathythermographs (AXBTs) which are instruments that measure the ocean temperature with depth (Boyd, 1987). To obtain turbulence-quality winds, starting in 2023 the sUAS have a MHPP on the nose of the aircraft (in addition to a pitot tube) which allows for obtaining high-frequency measurements of three-dimensional winds. The sUAS flown for this study is a Black Swift Technologies (BST) S0 (discussed in Section 2). A clear air data collection mission for the S0 occurred on 24 March 2023. The overall purposes of this mission were to: (a) demonstrate the ability of the S0 to survive and fly after being launched out of the P-3, (b) demonstrate the battery life of the S0, (c) verify the performance of the meteorological sensors, and (d) verify the S0's ability to fly near the ocean surface. Consistent with the fourth objective, near the end of the mission, the S0 was able to maintain a roughly 10-m altitude above the surface of the ocean for approximately 23.0 min (12.7 min of straight leg paths) in wind speeds below 10 m s^{-1}. To the authors' knowledge, this is the first time an air-deployed sUAS has flown close to the ocean surface for an extended period. While not in the high wind TC region, this paper demonstrates the versatility of using sUAS to sample the low

10.1029/2025EA004305

23335084, 2025, 8, Downloaded from https://agupubs.onlinelibrary.wiley.com/doi/10.1029/2025EA004305 by Battelle Memorial Institute, Wiley Online Library on [02/09/2025]. See the Terms and Conditions (https://onlinelibrary.wiley.com/terms-and-conditions) on Wiley Online Library for rules of use; OA articles are governed by the applicable Creative Commons License

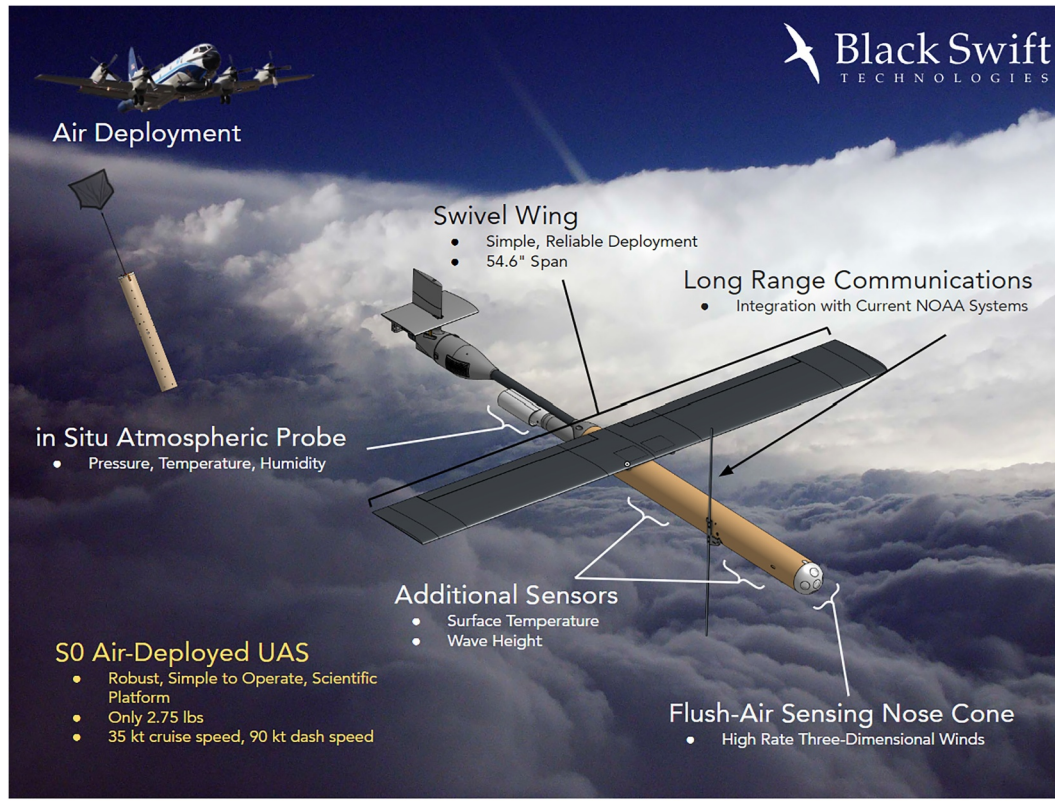

Figure 1. A schematic description of the Black Swift S0 and its deployment from the NOAA P-3.

levels of the atmospheric marine boundary layer and how the measurements can be used to estimate exchange coefficients.

The rest of the paper is organized as follows. Section 2 describes the BST S0 configuration, and the methods used to calculate the exchange coefficients. Section 3 discusses the measurements taken by the S0 and how the derived coefficients compare to previous studies. Section 4 summarizes the results and discusses next steps.

2. Data and Methodology

2.1. Description of the BST S0 sUAS

The S0 is a 1.58 kg (~3 pound) sUAS manufactured by BST that NOAA has been working toward deploying into hurricanes since it was awarded a Small Business Innovative Research (SBIR) award in 2018. This sUAS has a cruise speed of 22.5 m s^{-1}, a wingspan of 1.38 m, a maximum battery life of ~1.5 hr, and a maximum altitude of ~4,600 m. The S0 can fly at GPS altitude as well as at pressure altitude. To maintain a relatively constant altitude, the BST S0 is equipped with a laser altimeter that activates when the aircraft is below 300 ft (~91 m).

The S0 launches out of the standard A-sized sonobuoy cute on the P-3 and utilizes the SwiftCore Flight Management System by BST. The S0's wings are folded prior to launch such that the whole sUAS fits into a cylindrical container that is attached to a parachute (Figure 1). Once released from the P-3, the parachute deploys which slows down the cylindrical container and the S0 can slide out and the fly. The S0 typically recovers to controlled flight within 1,500 ft of the deployment altitude. With the missions over water, the S0 communicates data back to the P-3 using a two-way radio and is non-recoverable once the battery runs out.

The nose of the S0 contains a 5-hole MHPP capable of measuring winds up to 100 Hz (with all other measurements being recorded up to 10 Hz) that is also manufactured by BST. Due to bandwidth limitations of the antenna on the P-3, as well as the recording of engineering data for BST in the data stream, wind measurements (as well as pressure, temperature, and humidity measurements) were transmitted at ~4 Hz during the 24 March

23335084, 2025, 8, Downloaded from https://agupubs.onlinelibrary.wiley.com/doi/10.1029/2025EA004305 by Battelle Memorial Institute, Wiley Online Library on [02/09/2025]. See the Terms and Conditions (https://onlinelibrary.wiley.com/terms-and-conditions) on Wiley Online Library for rules of use; OA articles are governed by the applicable Creative Commons License

2023 mission described later in this manuscript. While always trying to improve, this was the highest frequency possible while still transmitting aircraft health, and providing enough of a gap to wait for any commands from the ground station.

The MHPP for the air-deployed S0 was calibrated at the Embry-Riddle Aeronautical University (ERAU) wind tunnel during February 2023 with a methodology following Kjelgaard (1988), van den Kroonenberg et al. (2008), and Wildmann et al. (2014). The air pressure, temperature, and humidity sensors used in the S0 are the Vaisala RSS421 sensor package, which has the sensors used on RD41 dropsondes and has previously been adapted for use both other sUAS (Cleary et al., 2022; de Boer et al., 2022, 2024). As described by Cleary et al. (2022), the Vaisala RSS421 sensors have been validated using a RS41 radiosonde (which has a nearly identical setup as the RSS421) at 1,000 hPa when moving at 6 m s^{-1}. The temperature sensor has a linear resistive platinum temperature sensor with a resolution of 0.01°C, repeatability of 0.1°C, and response time of 0.5 s. The humidity sensor includes a thin-film capacitor with a resolution of 0.1 % RH and a repeatability of 2 % RH, with a temperature-dependent response time of better than 0.3 s at 20°C. The pressure sensor is capacitive with a silicon diaphragm, having a resolution of 0.01 hPa and a repeatability of 0.4 hPa. Validation of the S0 meteorological measurements is discussed in the next section.

2.2. Verification of the Black Swift Technologies S0 Wind Measurements

Since it is difficult to verify the accuracy of the S0 measurements over the open ocean, wind measurements from the S0 were validated against Atmospheric Radiation Measurement's Southern Great Plains (SGP) 60 m wind tower (Cook, 2016) in Lamont, Oklahoma between 29 March and 3 April 2021. The SGP tower includes a 3D sonic anemometer, providing fast measurements of horizontal and vertical wind components. Additionally, it includes temperature and humidity measurements. The site also includes a variety of remote sensors. Over the course of 3 days at the SGP site, the S0 completed 10 flights providing meteorological data. The performance of the S0 compared to another commercially available sUAS as well as three university-developed research systems during that time was evaluated by De Boer et al. (2024). De Boer et al. found that the S0 provided reasonable measurements of the state of the atmosphere and demonstrated the sUAS's ability to measure momentum and sensible heat fluxes, though every sUAS tested had errors compared to the SGP wind tower. The biases in the S0 from the SGP flights have since been addressed by changing the sensor setup and including a new shroud that limits solar influence on the temperature and humidity measurements. These flights at the SGP wind tower leveraged a variety of flight patterns to allow for evaluation of the system's wind and thermodynamic sensing capabilities. For example, Figure 2 shows the time series of wind measurements for 10 S0 flights against the weather tower instrument at 60 m. For all 10 flights in Figure 2, the sUAS was generally within 1 km horizontal distance from the SGP tower flying at near 60 m altitude. For all three wind components, the mean differences of average wind speed and standard deviation of wind speed for all 10 flights are given in Table 1. The average wind components measured by the S0 were all within 0.50 m s^{-1} of that measured by the SGP tower. Importantly, while there can be biases either due to instrument error or due to the S0 sampling slightly different air than the wind tower, the S0 reports similarly shaped histograms of the wind speed for all three wind components (Figure 3). Additionally, measurements of the wind components from the S0 have a standard deviation within 0.61 m s^{-1} of that of the SGP site (Table 1). Results from Figure 3 and Table 1 yield confidence in the platform's ability to measure turbulence-scale variations in wind velocities.

We also evaluate the data for the mission on 24 March 2023 analyzed in this study. Before the S0 flew at near 10 m altitude, it performed a box pattern at 1,219 m (4,000 ft) with 5 km legs to determine if the wind reported any biases when flying in different orientations with respect to the prevailing wind (Figure 4). To validate the data, after the S0 flew the box pattern at 1,219 m and descended, the P-3, which performed a wind calibration flight prior to our S0 testing, descended to 1,219 m and flew the same box pattern. Additionally, during the mission dropsondes were deployed ∼1 hr both before and after the S0 flew at 4,000 ft. Comparing sUAS data to dropsonde data can be difficult since sUAS does not strictly capture a single profile of the atmosphere as a dropsonde does. This means that dropsondes do not capture the inherent variability that is present in the atmosphere and only show a single point from when they passed through the altitude that the S0 flew. Thus, the best way to validate these over-ocean sUAS measurements is to ensure that they are within bounds set by other measurements taken both before and after the sUAS flew.

23335084, 2025, 8, Downloaded from https://agupubs.onlinelibrary.wiley.com/doi/10.1029/2025EA004305 by Battelle Memorial Institute, Wiley Online Library on [02/09/2025]. See the Terms and Conditions (https://onlinelibrary.wiley.com/terms-and-conditions) on Wiley Online Library for rules of use; OA articles are governed by the applicable Creative Commons License

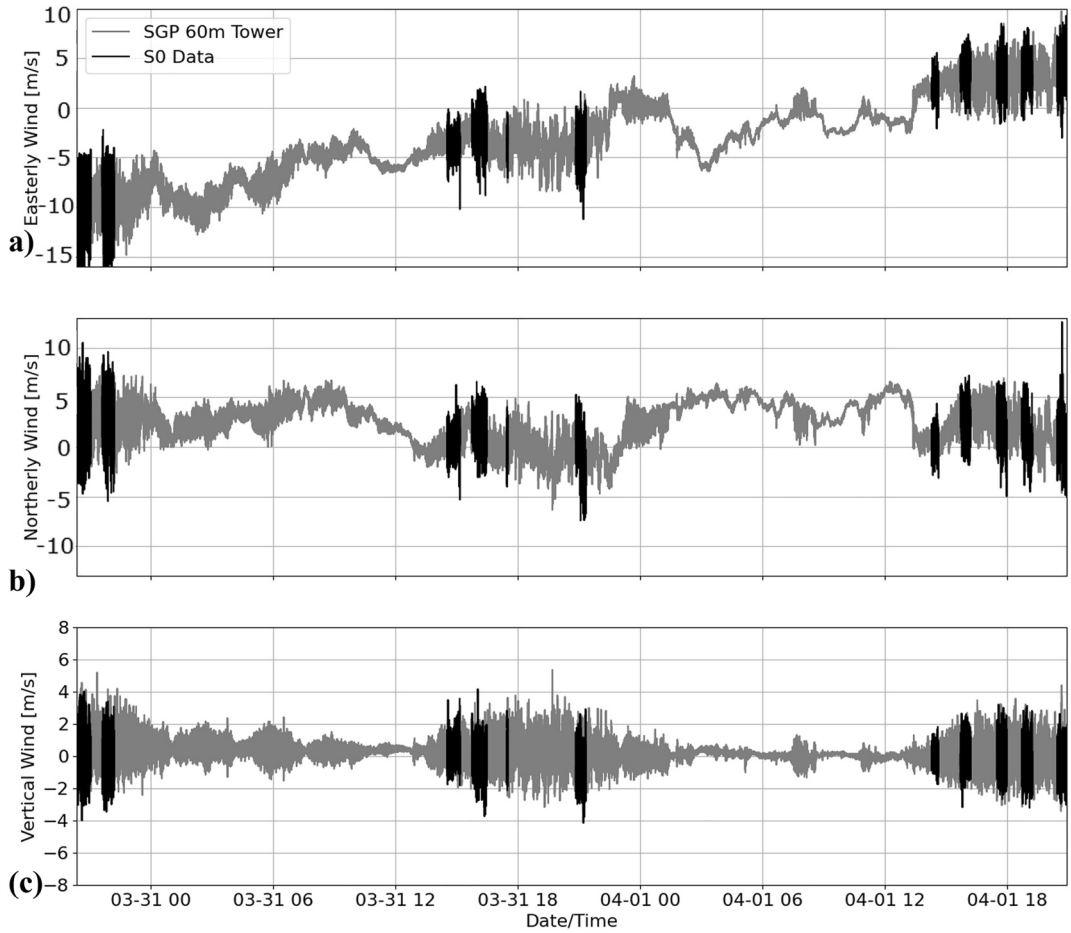

Figure 2. Time series of (a) Easterly (zonal wind), (b) Northerly (meridional wind), and (c) vertical (w) wind of the 10 S0 flights versus the SGP tower instrument at 60 m.

Generally, all of the variability of the horizontal wind measurements from the S0 are captured by the dropsonde and P-3 flight-level measurements (Figures 5a and 5b). Of note, the vertical wind speed is too variable over time and space to have a meaningful quantitative comparison between the measurement platforms. Over the course of ~2.5 hr from the first to last dropsonde measurement, the wind speed ranged between 4.34 and 6.58 m s^{-1} while the wind direction ranged between 226 and 236°. The peaks in wind speed and wind direction occur during turns which are excluded from the analysis of the data at low levels (discussed further below). Both air temperature (Figure 5c) and relative humidity (Figure 5d) data from the S0 had reasonable mean values and variability during this mission, as compared to dropsonde and P-3 flight-level data. The lack of S0 measurement-dependency on the wind-relative direction of the aircraft motion was confirmed as the largest difference between leg-averaged wind speed, wind diction, temperature, and relative humidity was 0.31 m s^{-1}, 0.53 deg, 0.74°C, and 4.92%, respectively. Of note, the P-3 flight-level RH had questionable values and should be interpreted with caution. Discussion with engineers for the P-3 indicated a potential electrical signal interfering with the hygrometer. Additionally, the

Table 1
An Evaluation of the Differences in Mean Wind Speed and Standard Deviation of the Wind Speed Between the S0 and the SGP Tower for All 10 Missions Shown in Figure 2

	Easterly wind (u)	Northerly wind (v)	Vertical wind (w)
Mean difference in the mean wind speed for the 10 SGP flights (m/s)	0.50	0.34	0.39
Mean difference in the standard deviation of the wind speed for the 10 SGP flights (m/s)	0.50	0.61	0.13

10.1029/2025EA004305

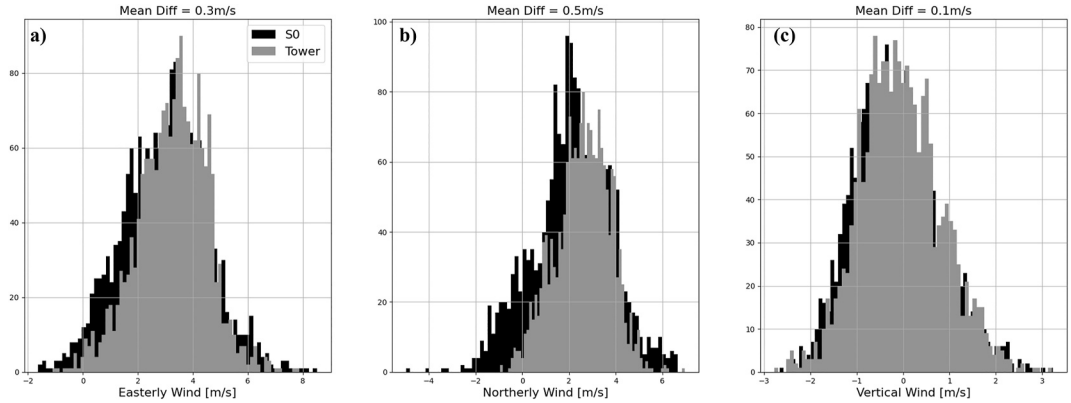

Figure 3. A histogram comparison of the (a) Easterly (zonal), (b) Northerly (meridional), and (c) Vertical components of the wind for the ninth S0 flight near the SGP tower. Binning in all panels is 0.05 m s^{-1}.

P-3 flight-level sensors were not calibrated prior to this mission which led to questionable variability along some of the legs. To avoid potential issues with these fluctuations, we only show the mean values in Figure 5.

2.3. Determining the Air-Sea Exchange Coefficients

The location of the mission and flight path over the low-level portion of the S0 mission is given in Figure 6. The location indicated in Figure 6 is on the western edge of a high-pressure region (not shown) which indicates generally southerly wind at the location of the mission. Start and end times for each leg were manually determined for when the S0 was flying in a straight line (i.e., turns were removed) and resulted in leg lengths of ∼2.15 km. The flight pattern was designed such that the S0 flew with both a head wind and a tail wind. The prevailing wind direction was determined using dropsonde data ∼20 min before the S0 started this part of the flight. A total of 8 paths were analyzed (4 into the wind and 4 against the wind). A mean value of every scalar quantity was determined for each leg which were used to determine momentum, heat, and moisture flux values for those legs. The flight times for each leg is given in Table 2. For legs 3, 4, 6, and 8, we subjectively identified that the hygrometer had a delay in reaching equilibrium. When calculating latent heat flux and sensible heat flux for each of these legs, the beginning of the legs were shortened to ensure that biases resulting from the aircraft turning were not included as part of the analysis. Through subjective analysis, we have determined that airflow to the sensors during sharp turns can be suboptimal. The lengths of the shortened legs are also given in Table 2.

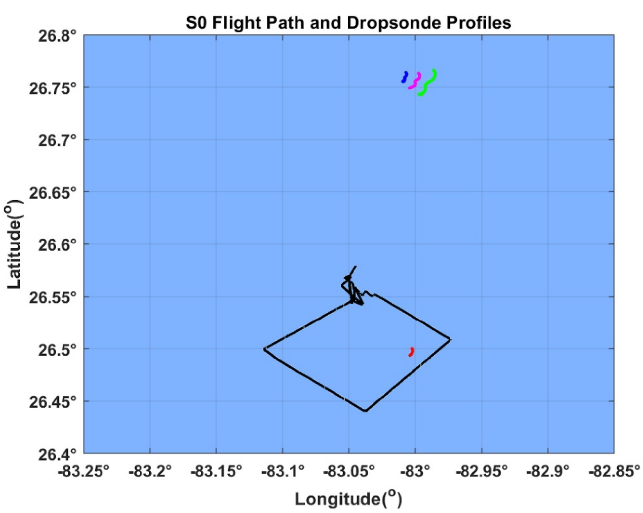

Figure 4. The horizontal trajectory of the S0 (black) and the dropsondes (other colors) for the mission on 24 March 2023.

With the goal of validating quality of the measurements, Figure 7 shows an averaged spectral analysis of the winds measured by the S0 during the 8 legs identified in Table 2. The power spectral density from all three Cartesian velocity components (Figures 7a–7c) show that most data follow the −5/3 power law between 0.03 HZ to 1 Hz, consistent with other studies using aircraft velocity data (e.g., Zhang et al., 2010; Zhao et al., 2020).

To be consistent with classical boundary layer studies, we break down the winds into the along-wind and cross-wind components. Following the methodology of French et al. (2007), the averaged cumulative covariance (Figure 7d) shows linear growth indicating a relatively uniform flux distribution along the flight paths. The cospectra of those components (Figure 7e), computed show that the larger-scale structures with a frequency near 0.03 Hz provide the dominant downward momentum transport, especially for the cross-wind component. Using Taylor's Frozen Hypothesis, we covert this frequency to a wavelength of ∼750 m (wavelength is equal to aircraft velocity divided by the frequency) using an aircraft velocity of 22.5 m s^{-1}. Of note, while we show similar magnitudes of measured turbulent flux in the along-wind and cross-wind directions, some prior studies have shown that there are higher amounts of turbulent flux in the along-wind direction.

23335084, 2025, 8, Downloaded from https://agupubs.onlinelibrary.wiley.com/doi/10.1029/2025EA004305 by Battelle Memorial Institute, Wiley Online Library on [02/09/2025]. See the Terms and Conditions (https://onlinelibrary.wiley.com/terms-and-conditions) on Wiley Online Library for rules of use; OA articles are governed by the applicable Creative Commons License

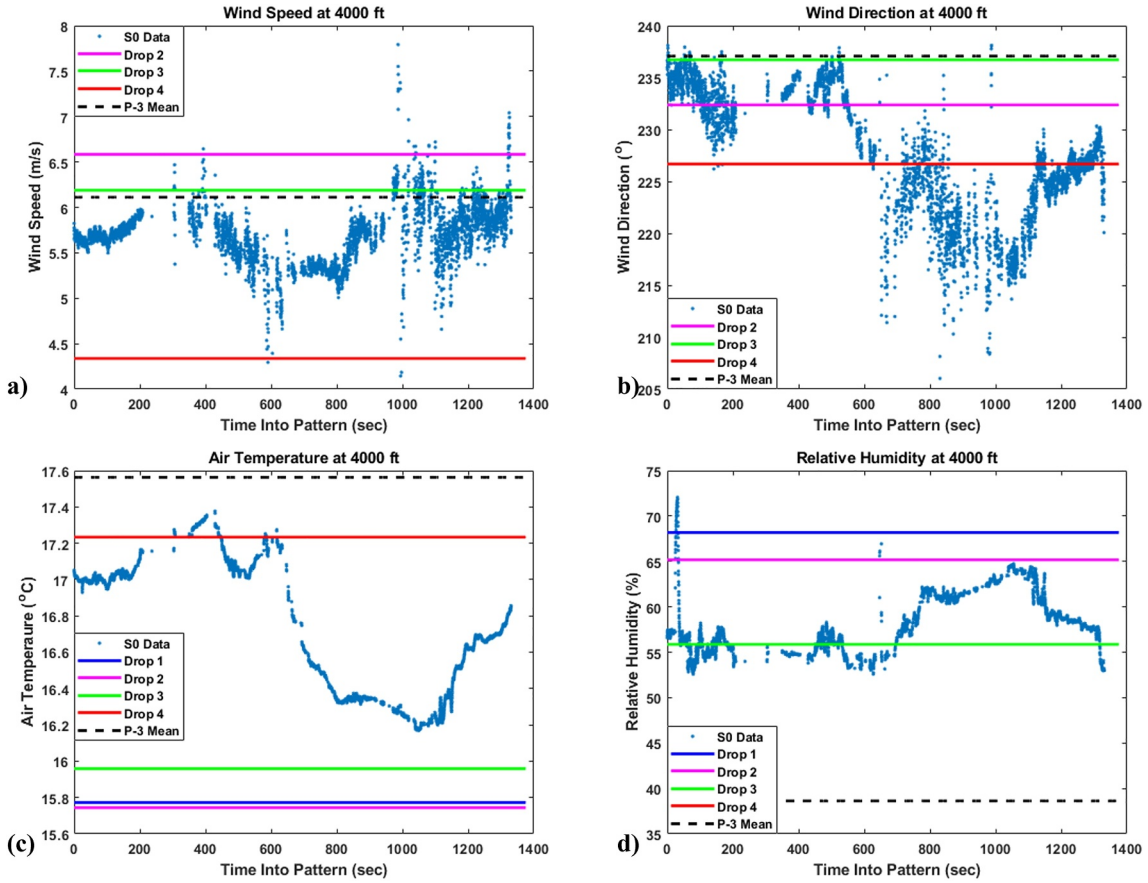

Figure 5. A comparison of (a) wind speed, (b) wind direction, (c) air temperature, and (d) relative humidity between the S0 while it was at 4,000 ft altitude, four dropsondes that passed through that altitude, and the mean value from the P-3 as it flew the same pattern as the S0 at 4,000 ft. Gaps in S0 data were due to temporary reduction in coms quality. Note that Drop 1 did not report any wind data and Drop 4 did not report relative humidity data at 4,000 ft. The time the S0 was at 4,000 ft was between 22:51 and 23:14 UTC while Drop 1 was deployed at 21:22 UTC, Drop 2 at 21:27 UTC, Drop 3 at 21:57 UTC, and Drop 4 at 23:59 UTC. The P-3 flew the box pattern between 23:39 and 24:00 UTC.

The cumulative cospectral sums, or "ogives," are shown in Figure 7f. The ogive plots have been widely used in turbulence studies to determine useful time intervals suitable for turbulent flux calculations (e.g., French et al., 2007; Zhang et al., 2010; Zhao et al., 2020). When ogives asymptotically approach a single value, the homogeneity assumption for Reynolds Averaging is met. In Figure 7f, both along-wind and cross-wind ogives

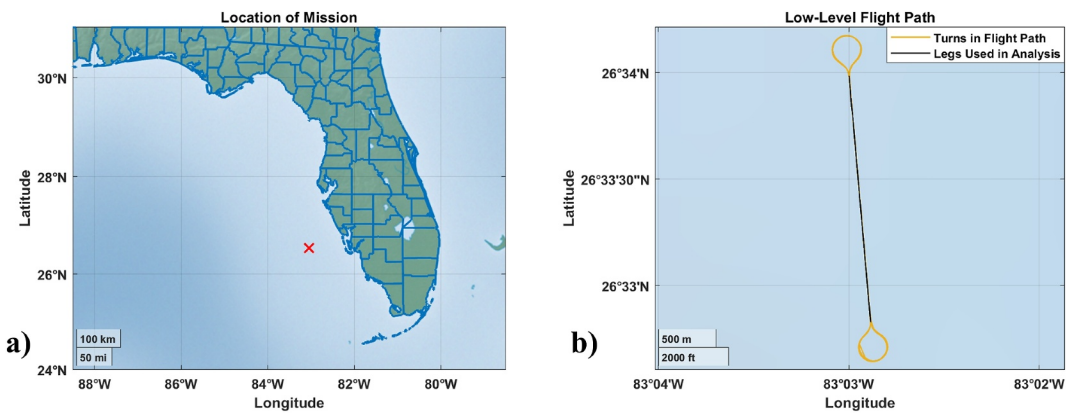

Figure 6. The location of the mission off the west coast of Florida on 24 March 2023, at 22Z, (b) The flight path of the S0 during the low-level portion of the flight. In (b) the yellow portion of the flight pattern was identified as a turn and not included in the legs.

23335084, 2025, 8, Downloaded from https://agupubs.onlinelibrary.wiley.com/doi/10.1029/2025EA004305 by Battelle Memorial Institute, Wiley Online Library on [02/09/2025]. See the Terms and Conditions (https://onlinelibrary.wiley.com/terms-and-conditions) on Wiley Online Library for rules of use; OA articles are governed by the applicable Creative Commons License

Table 2
The Flight Time for Each Leg

Flight leg number	Time of leg in seconds (time for legs with hygrometer delay)
1	118.4
2	80.2
3	116.9 (109.3)
4	80.1 (52.9)
5	116.2
6	78.5 (54.5)
7	92.6
8	81.0 (55.7)

Note. For legs 3, 4, 7, and 8 the time used to calculate the latent heat flux is in parentheses. The full leg lengths are 2.15 km.

meet this criteria ~0.2 Hz or ~112.5 m for small eddies. This is not fully met for large eddies near 0.02 Hz or 1,225 m which is the Nyquist frequency of the legs. While it would be ideal to have longer legs to sample larger eddies, we still have confidence that we are sampling the majority of the spectra of turbulent energy.

With a goal of calculating the air-sea 10 m neutral drag coefficient (C_{DN}), we followed a methodology described by Andreas et al. (2012) and Vickers et al. (2013), who also used the direct eddy-covariance method for aircraft measurements. We adjust the winds to 10 m and to a neutral stability boundary layer using Equation 1 which depends on the measured mean winds U at height z, the surface friction velocity u_* (Equation 2), the von Karman constant, $\kappa = 0.4$, and the stability function for momentum ψ_m (Equation 3). In all the equations, overbars represent time means and primes denote deviations from the mean. The average GPS altimeter reading over all 8 legs was 10.14 m above the surface of the ocean. However, the laser altimeter (which is sensitive to ocean wave height) showed a mean altitude of 15.1 m above the ocean surface. For all the calculations in this study we use the height from the laser altimeter.

$$U_{10N} = U(z) - \left(\frac{u_*}{\kappa}\right)\ln\left(\frac{z}{10}\right) + \left(\frac{u_*}{\kappa}\right)\psi_m, \tag{1}$$

$$u_* = \left(\overline{w'u'}^2 + \overline{w'v'}^2\right)^{1/4}, \tag{2}$$

$$\psi_m(\zeta) = \begin{cases} 2\ln\left(\frac{1+x}{2}\right) + \ln\left(\frac{1+x^2}{2}\right) - 2\tan^{-1}(x) + \frac{\pi}{2}; & \zeta < 0 \\ -5\zeta; & \zeta > 0 \end{cases} \tag{3}$$

$$L \equiv \frac{-u_*^3\,\overline{\theta_v}}{(g\kappa)\left(\overline{w'\theta_v'}\right)}, \tag{4}$$

For the stability criteria in Equation 3, $x = (1 - 16\zeta)^{1/4}$ where $\zeta = z/L$ and L is the Obukhov length scale defined in Equation 4 where, $g = 9.81$ m s^{-2} is the acceleration due to gravity, w is vertical velocity, and θ_v is virtual potential temperature (Businger, 1966; Businger et al., 1971; Dyer, 1974; Högström, 1988; Paulson, 1970). In Equation 3, a negative value for ζ is for an unstable atmosphere and a positive value is for a stable atmosphere. To obtain the equivalent neutral value 10 m values for q and θ, a similar process is undergone in Equations 5 and 6 where q_* and θ_* are flux scales analogous to u_* and are given by

$$q_{10N} = q(z) - \left(\frac{q_*}{\kappa}\right)\ln\left(\frac{z}{10}\right) + \left(\frac{q_*}{\kappa}\right)\psi_E, \tag{5}$$

$$\theta_{10N} = \theta(z) - \left(\frac{\theta_*}{\kappa}\right)\ln\left(\frac{z}{10}\right) + \left(\frac{\theta_*}{\kappa}\right)\psi_H, \tag{6}$$

23335084, 2025, 8, Downloaded from https://agupubs.onlinelibrary.wiley.com/doi/10.1029/2025EA004305 by Battelle Memorial Institute, Wiley Online Library on [02/09/2025]. See the Terms and Conditions (https://onlinelibrary.wiley.com/terms-and-conditions) on Wiley Online Library for rules of use; OA articles are governed by the applicable Creative Commons License

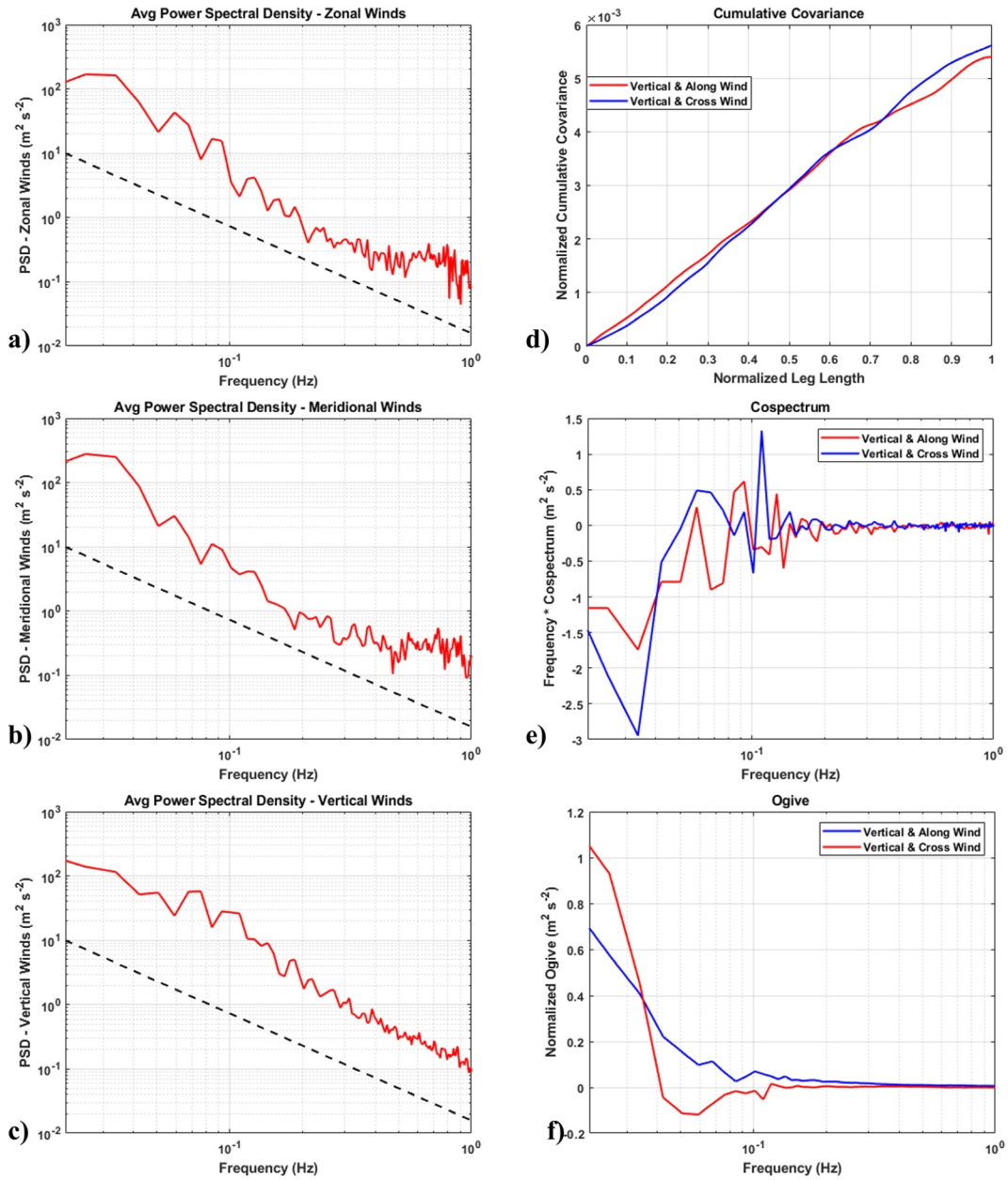

Figure 7. (a–c) average power spectral density of the zonal, meridional, and vertical velocities, respectively, measured from the S0 during the 8 legs. In each plot a −5/3 reference line is shown. (d) Average cumulative covariance of the along-wind and cross-wind components as a function of leg length (d, e) average cospectrum and ogives, respectively, of the along-wind and cross-wind components of the wind over the 8 legs. Both plots in (d, e) start at the Nyquist frequency of $2.09*10^{-2}$ Hz.

where q is specific humidity, θ is potential temperature, $q_* = -\frac{\overline{w'q'}}{u_*}$ and $\theta_* = -\frac{\overline{w'\theta'}}{u_*}$. A common assumption is that $\psi_E = \psi_H$ (e.g., Abbasi et al., 2017). For the case of a stable atmosphere (i.e., $\zeta > 0$), ψ_E and ψ_H are the same as ψ_m in Equation 3. In the unstable atmosphere, the stability function for heat and moisture is given by Equation 7.

$$\psi_H(\zeta) = \psi_E(\zeta) = 2 * \ln\left(\frac{1+x^2}{2}\right); \zeta < 0 \tag{7}$$

The 10 m neutral values of wind, temperature, and humidity are used to determine the exchange coefficients of momentum, heat, and moisture at the air-sea interface. The wind stress (or momentum flux) is given by

23335084, 2025, 8, Downloaded from https://agupubs.onlinelibrary.wiley.com/doi/10.1029/2025EA004305 by Battelle Memorial Institute, Wiley Online Library on [02/09/2025]. See the Terms and Conditions (https://onlinelibrary.wiley.com/terms-and-conditions) on Wiley Online Library for rules of use; OA articles are governed by the applicable Creative Commons License

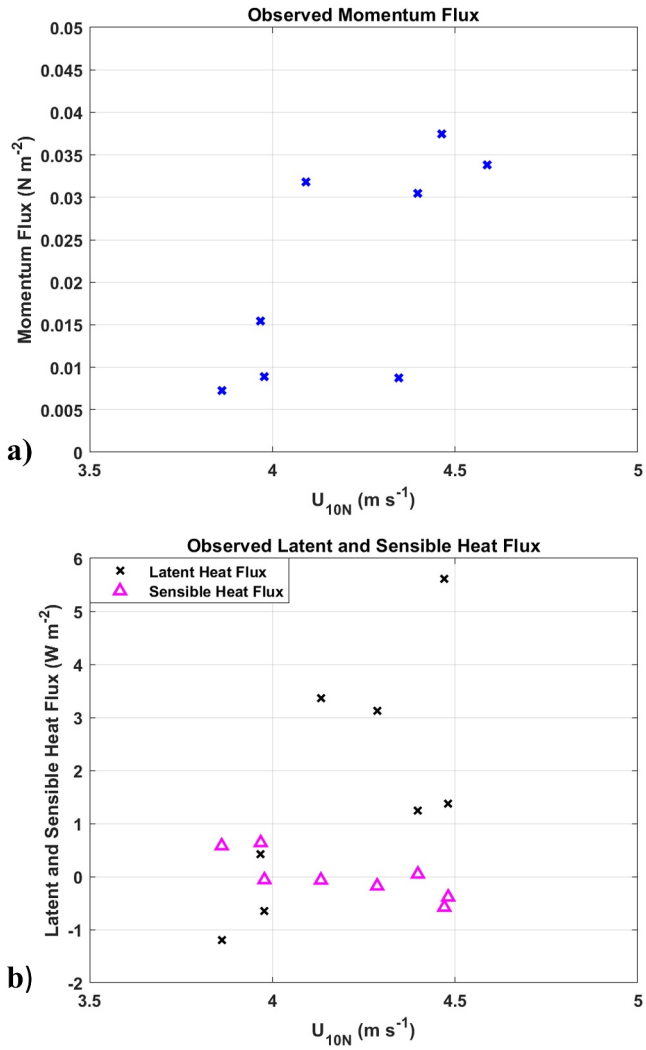

Figure 8. A comparison of neutral 10 m neutral wind speed with (a) momentum flux (b), sensible heat flux and latent heat flux, each calculated for the 8 flight path legs.

Equations 8 and 9 where Equation 8 represents the direct eddy covariance definition and Equation 9 represents the bulk aerodynamic formula where ρ is the air density and C_{DN} is the neutral 10 m drag coefficient. With all other variables measured by the sUAS or derived from Equation 1, C_{DN} is solved for in Equation 10.

$$\tau = -\rho\left[\overline{u'w'}^2 + \overline{u'w'}^2\right]^{1/2} \tag{8}$$

$$\tau = \rho C_{\mathrm{DN}} U_{10N}^2 \tag{9}$$

$$C_{\mathrm{DN}} = \frac{\left[\overline{u'w'}^2 + \overline{v'w'}^2\right]^{1/2}}{U_{10N}^2} \tag{10}$$

A similar process is done for turbulent sensible heat transfer which is shown by Equations 11–13 where F_H is the sensible heat flux, $c_p = 1004\ \mathrm{J\ kg^{-1}\ K^{-1}}$ is the specific heat of air at constant pressure, C_{HN} is the neutral sensible heat flux transfer coefficient, θ_o is the potential temperature using the sea surface temperature (SST), and θ_{10N} is the neutral potential temperature of the air at 10 m above the surface of the ocean given by Equation 6. A SST of 22.9°C was measured by an AXBT released during the S0 mission (S0 recorded ~22.7°C SST using an infrared sensor). The SST measurement was also corroborated by a dropsonde with an attached infrared sensor (Zhang et al., 2017).

$$F_H = \rho c_p \overline{\theta' w'} \tag{11}$$

$$F_H = \rho c_p C_H U_{10N}(\theta_0 - \theta_{10N}) \tag{12}$$

$$C_{HN} = \frac{\overline{\theta' w'}}{U_{10N}(\theta_0 - \theta_{10N})} \tag{13}$$

Equations 14–16 show the results for turbulent latent heat transfer where $L_v = 2.5 \times 10^6\ \mathrm{J\ kg^{-1}}$ is the latent heat of vapourization, F_E is the latent heat flux, C_{EN} is the neutral latent heat flux transfer coefficient, q_0 is the specific humidity of the surface of the ocean which assumes 98% saturation, and q_{10N} is the neutral specific humidity at 10 m above the surface of the ocean from Equation 5.

$$F_E = \rho L_V \overline{q' w'} \tag{14}$$

$$F_E = \rho L_V C_{\mathrm{EN}} U_{10N}(q_0 - q_{10N}) \tag{15}$$

$$C_{\mathrm{EN}} = \frac{\overline{q' w'}}{U_{10N}(q_0 - q_{10N})} \tag{16}$$

3. Results

On all 8 flight legs, the S0 measured the mean 10 m neutral wind speeds between 3.86 m $\mathrm{s^{-1}}$ and 4.48 m $\mathrm{s^{-1}}$. The extracted momentum flux values using the direct eddy correlation method ranged from 7.24×10^{-3} N $\mathrm{m^{-2}}$ to 3.74×10^{-2} N $\mathrm{m^{-2}}$ (Figure 8a). The eddy correlation derived latent heat fluxes display a larger range of results than that of the sensible heat flux for the same 10 m neutral wind speeds (Figure 8b). Latent heat flux ranged between −1.19 W $\mathrm{m^{-2}}$ and 5.61 W $\mathrm{m^{-2}}$, while sensible heat flux ranged between −0.58 W $\mathrm{m^{-2}}$ and 0.64 W $\mathrm{m^{-2}}$.

23335084, 2025, 8, Downloaded from https://agupubs.onlinelibrary.wiley.com/doi/10.1029/2025EA004305 by Battelle Memorial Institute, Wiley Online Library on [02/09/2025]. See the Terms and Conditions (https://onlinelibrary.wiley.com/terms-and-conditions) on Wiley Online Library for rules of use; OA articles are governed by the applicable Creative Commons License

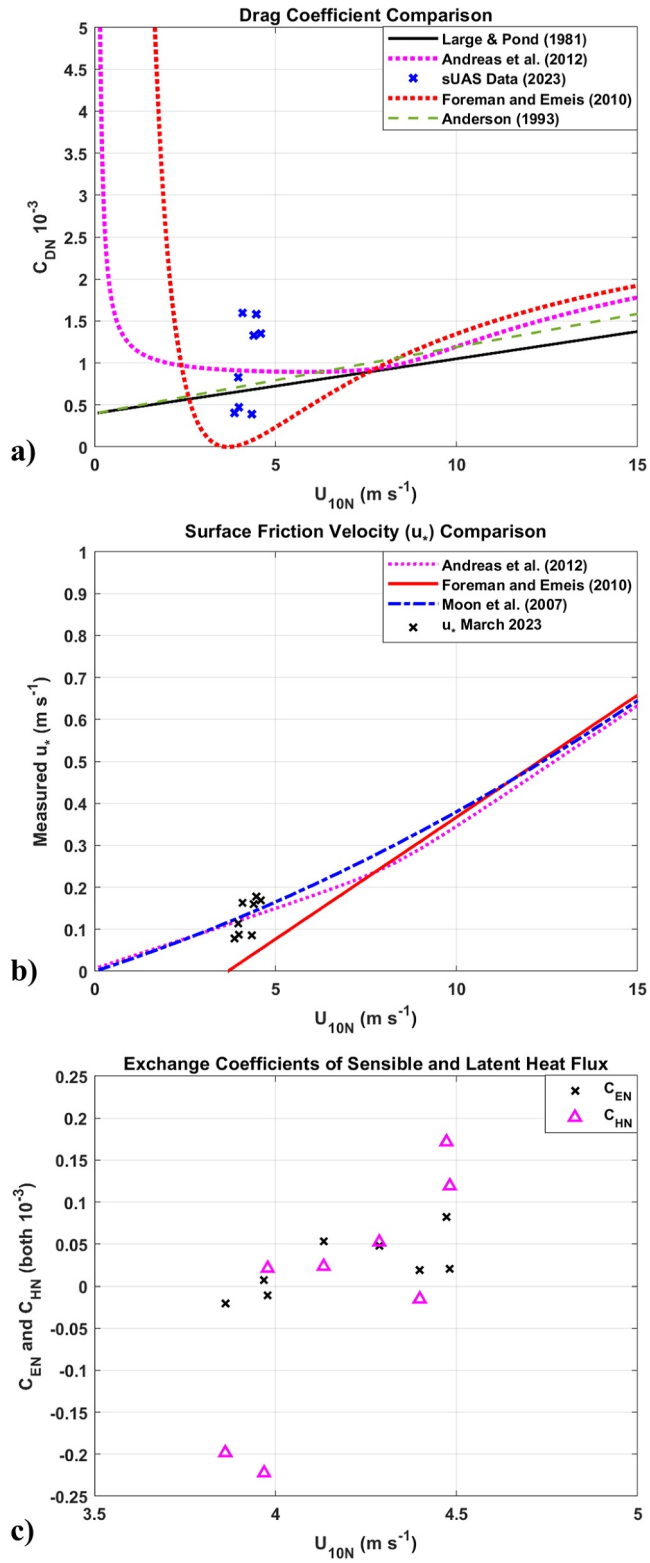

Figure 9. A comparison of 10 m neutral wind speed with (a) drag coefficient C_{DN}, (b) a comparison of 10 m neutral wind speed with u_*, (c) exchange coefficient of sensible heat C_{HN} and the exchange coefficient of latent heat C_{EN}, each calculated for the 8 flight path legs. Of note, the x-axis range in (a) is different than that in (c) in order to facilitate comparison with previous studies.

23335084, 2025, 8, Downloaded from https://agupubs.onlinelibrary.wiley.com/doi/10.1029/2025EA004305 by Battelle Memorial Institute, Wiley Online Library on [02/09/2025]. See the Terms and Conditions (https://onlinelibrary.wiley.com/terms-and-conditions) on Wiley Online Library for rules of use; OA articles are governed by the applicable Creative Commons License

23335084, 2025, 8, Downloaded from https://agupubs.onlinelibrary.wiley.com/doi/10.1029/2025EA004305 by Battelle Memorial Institute, Wiley Online Library on [02/09/2025]. See the Terms and Conditions (https://onlinelibrary.wiley.com/terms-and-conditions) on Wiley Online Library for rules of use; OA articles are governed by the applicable Creative Commons License

Figure 9 shows the derived coefficients of C_{DN}, C_{HN}, and C_{EN}, that were calculated by equating the direct covariance measurements with the respective equations for the bulk aerodynamic formulas of momentum flux (Equation 10), sensible heat flux (Equation 13), and latent heat flux (Equation 16). The values for the coefficients were calculated using the same range for neutral 10 m wind speeds as in Figure 8. The derived values of C_{DN} for the eight legs ranged between 0.39×10^{-3} and 1.60×10^{-3} (Figure 9a). The range of derived C_{DN} values displayed here is within the range of values derived in previous observational studies at similar wind speeds (e.g., Anderson, 1993; Foreman & Emeis, 2010; Large & Pond, 1982). Even with only eight values, the mean value of C_{DN} across the eight flight legs was 0.99×10^{-3} which is within a 10 percent difference from the value of 0.907×10^{-3} predicted by the final function given by Andreas et al. (2012) at the same U_{10N} of 4.21 m s^{-1}. While the measurements in this study were taken on a calm day, the variability in C_{DN} may be explained by differing sea state conditions such as wave height, wave slope, wave period, and wave age which have been shown to have an impact on momentum transfer (e.g., Herbach, 2011; Högström et al., 2009; Mueller & Veron, 2009; Moon et al., 2007). Some studies have shown that changes to the sea state can have a greater impact on the drag coefficient magnitude than the wind speed (e.g., Edson et al., 2013; Holthuijsen et al., 2012; Johnson et al., 1998; Reichl et al., 2014; Smith et al., 1992; Taylor & Yelland, 2001; Toba et al., 1990; Zhou et al., 2022). The inclusion of sea-states in the analysis of C_{DN} was previously brought up in Andreas et al. (2012) as well as showing u_* alongside U_{10N} to remove the uncertainty of C_{DN} in low winds (see Figure 9b). If the data set of sUAS data to calculate C_{DN} becomes large enough collocated with P-3 and/or buoy-based wave observations, potential future work is to also make C_{DN} a function of sea-state variables such as wave height, wave slope, wave period, and wave age which have been shown to have an impact on momentum transfer.

The magnitudes of C_{EN} and C_{HN} are significantly lower (by ~2 orders of magnitude) than those in previous studies at wind speeds between 5 m s^{-1} and 25 m s^{-1} which found values closer to 1.0×10^{-3} (e.g., Anderson, 1993; DeCosmo et al., 1996; Edson, 2013; Large & Pond, 1982; Zou et al., 2017). Additionally, few studies have derived negative value of C_{HN} and C_{EN}. However, Oost et al. (2000) found this to be possible in a unique atmospheric state where the Obukhov length scale, L, is negative indicating an unstable stratification (buoyant processes dominate shear production in the production of turbulent kinetic energy), but the potential temperature of air at 10 m is higher than potential temperature of the ocean surface indicating a stable stratification. Oost et al. (2000) found that in this "semi-unstable" atmosphere, C_{HN} and C_{EN} can be lower than in other atmospheric states (see their Figure 6). The data collected by the S0 during this mission meet the semi-unstable criteria.

With the lack of available data, it is a common assumption that $C_{EN} = C_{HN}$. Komori et al. (2018) summarizes the values of C_{EN}, C_{HN}, and C_{KN} (the exchange coefficient for enthalpy) in their study, as well as that from Bell et al. (2012), Jeong et al. (2012), and Richter and Stern (2014). In general, all those studies find that in winds less than 35 m s^{-1}, C_{EN} and C_{HN} closely match one another and are nearly constant. When winds are greater than 35 m s^{-1} C_{EN} and C_{HN} increase proportionally to U_{10N}. While only over a limited range of wind speed, the trend of C_{EN}, C_{HN} matches from those previous studies (albeit at a lower value as previously mentioned).

4. Conclusions

In this study, we presented the first ever direct measurements of momentum, latent heat, and sensible heat fluxes using a sUAS in the marine boundary layer. The sUAS measured these fluxes on 24 March 2023, in calm, clear conditions that were in a region of higher pressure off the west coast of Florida. The direct covariance measurements were set equal to the bulk aerodynamic formulae to derive the bulk transfer coefficients for momentum (C_{DN}), heat (C_{HN}), and moisture (C_{EN}).

The derived drag coefficient, C_{DN}, from the directly measured momentum fluxes ranged from 0.39×10^{-3} and 1.60×10^{-3} in mean 10 m neutral winds between 3.86 m s^{-1} and 4.48 m s^{-1}. These values of C_D are generally in good agreement with earlier studies that also had 10 m neutral wind speeds less than 10 m s^{-1} (e.g., Anderson, 1993; Andreas et al., 2012; Foreman & Emeis, 2010; Large & Pond, 1981). The mean derived C_{DN} of 0.99×10^{-3} is at 10 m neutral wind speed of 4.21 m s^{-1} and is within a 10 percent difference of the value derived using the function of Andreas et al. (2012) which predicted a value of 0.907×10^{-3} at the same neutral 10 m winds.

The derived latent heat exchange coefficient, C_{EN}, ranged between -0.020×10^{-3} and 0.082×10^{-3} while the derived sensible heat exchange coefficient, C_{HN}, ranged between -0.22×10^{-3} and 0.17×10^{-3} under the same 10 m neutral wind speed range as was used to derive C_{DN}. These are lower numbers than in previous studies that

23335084, 2025, 8, Downloaded from https://agupubs.onlinelibrary.wiley.com/doi/10.1029/2025EA004305 by Battelle Memorial Institute, Wiley Online Library on [02/09/2025]. See the Terms and Conditions (https://onlinelibrary.wiley.com/terms-and-conditions) on Wiley Online Library for rules of use; OA articles are governed by the applicable Creative Commons License

had values of C_{HN} and C_{EN} closer to 1.0×10^{-3} (e.g., Anderson, 1993; DeCosmo et al., 1996; Large & Pond, 1982). However, the low magnitudes of the heat coefficients are consistent with the rare conditions described by Oost et al. (2000) and observed in the current study which create a "semi-unstable" atmosphere. In these conditions, the Obukhov length scale L is negative (indicating an unstable atmosphere), but the atmosphere is statically stable. The heat transfer coefficients presented follow a similar trend as Komori et al. (2018), where the values of C_{HN} tend to be less than that of C_{EN} in lower mean 10 m neutral wind speeds ($U_{10N} \leq 10$ m s^{-1}). Due to the much lower number of previous studies surrounding the heat transfer coefficients in lower wind speeds, the comparison of the values calculated for C_{EN} and C_{HN} is more limited than the comparison of C_{DN}. To verify this explanation, for the discrepancy, more flights will be needed across multiple atmospheric states such as described by Oost et al. (2000).

The results presented provide the use and viability of sUAS, specifically the Black Swift Technologies S0, for studying air-sea interactions in the marine boundary layer. To obtain these air-sea fluxes, high frequency measurements are needed in the surface layer. Since it is too dangerous to fly crewed aircraft in surface layer, this research demonstrates how sUAS provide a viable alternative to obtain these crucial measurements. Lowering the uncertainty in the values of the exchange coefficients is crucial to improving operational numerical weather prediction models. For example, the ratio of C_K and C_{DN} is a crucial factor in determining TC intensity (i.e., Emanuel, 1986, 1995). With the ability to fly in the surface layer demonstrated, as well as the demonstrated ability of the S0 in high wind conditions (not shown), future work is to fly the S0 in the surface layer of tropical cyclones and derive the exchange coefficients in high wind environments.

Data Availability Statement

The sUAS data used in this manuscript is available on a public repository at Wadler (2024), https://doi.org/10.5281/zenodo.11397249.

Acknowledgments
We thank the generous support of NOAA's Uncrewed Systems Office (UxS) for funding some of these developments. Joshua Wadler also acknowledges support from the ERAU Faculty Innovative Research in Science and Technology (FIRST) Program and from NSF Award 2409475. Jun A. Zhang also acknowledges support from NOAA Grants NA22OAR4590174 and NA22OAR4590178, NSF Awards 2228299 and 2211308, and ONR MURI Grant N00014-24-1-2554. We especially thank all the hard work from the crew at AOC for helping to deploy the emerging technology such as the S0. We are grateful for the engineering faculty Drs. Gordon Leishman, Zheng Zhang, and Jim Gregory as well as student staff at ERAU for helping with the wind tunnel calibration missions.

References

Abbasi, A., Annor, F. O., & van de Giesen, N. (2017). Effects of atmospheric stability conditions on heat fluxes from small water surfaces in (semi-)arid regions. *Hydrological Sciences Journal*, *62*(9), 1422–1439. https://doi.org/10.1080/02626667.2017.1329587

Aberson, S. D., Zhang, J. A., Zawislak, J., Sellwood, K., Rogers, R., & Cione, J. J. (2023). The NCAR GPS dropwindsonde and its impact on hurricane operations and research. *Bulletin America Meteorology Social*, *104*(11), E2134–E2154. https://doi.org/10.1175/BAMS-D-22-0119.1

Anderson, R. J. (1993). A study of wind stress and heat flux over the open ocean by the inertial-dissipation method. *Journal of Physical Oceanography*, *23*(10), 2153–2161. https://doi.org/10.1175/1520-0485(1993)023<2153:ASOWSA>2.0.CO;2

Andreas, E. L., Mahrt, L., & Vickers, D. (2012). A new drag relation for aerodynamically rough flow over the ocean. *Journal of the Atmospheric Sciences*, *69*(8), 2520–2537. https://doi.org/10.1175/jas-d-11-0312.1

Bell, M. M., Montgomery, M. T., & Emanuel, K. A. (2012). Air–sea enthalpy and momentum exchange at major hurricane wind speeds observed during CBLAST. *Journal of the Atmospheric Sciences*, *69*(11), 3197–3222. https://doi.org/10.1175/JAS-D-11-0276.1

Black, P. G., D'Asaro, E. A., Drennan, W. M., French, J. R., Niiler, P. P., Sanford, T. B., et al. (2007). Air–sea exchange in hurricanes: Synthesis of observations from the coupled boundary layer air–sea transfer experiment. *Bulletin America Meteorology Social*, *88*(3), 357–374. https://doi.org/10.1175/bams-88-3-357

Boyd, J. (1987). Improved depth and temperature conversion equations for Sippican AXBTs. *Journal of Atmospheric and Oceanic Technology*, *4*(3), 545–551. https://doi.org/10.1175/1520-0426(1987)004<0545:IDATCE>2.0.CO;2

Businger, J. A. (1966). Transfer of momentum and heat in the planetary boundary layer. In *Proceedings of the Symposium on Arctic Heat Budget and Atmospheric Circulation, Lake Arrowhead* (pp. 305–332). The Rand Corporation.

Businger, J. A., Wyngaard, J. C., Izumi, Y., & Bradley, E. F. (1971). Flux-profile relationships in the atmospheric surface layer. *Journal of the Atmospheric Sciences*, *28*(2), 181–189. https://doi.org/10.1175/1520-0469(1971)028<0181:FPRITA>2.0.CO;2

Cione, J. J., Bryan, G. H., Dobosy, R., Zhang, J. A., de Boer, G., Aksoy, A., et al. (2020). Eye of the storm: Observing hurricanes with a small unmanned aircraft system. *Bulletin America Meteorology Social*, *101*(2), E186–E205. https://doi.org/10.1175/BAMS-D-19-0169.1

Cione, J. J., Kalina, E. A., Uhlhorn, E. W., Farber, A. M., & Damiano, B. (2016). Coyote unmanned aircraft system observations in Hurricane Edouard (2014). *Earth and Space Science*, *3*(9), 370–380. https://doi.org/10.1002/2016EA000187

Cleary, P. A., de Boer, G., Hupy, J. P., Borenstein, S., Hamilton, J., Kies, B., et al. (2022). Observations of the lower atmosphere from the 2021 WiscoDISCO campaign. *Earth System Science Data*, *14*(5), 2129–2145. https://doi.org/10.5194/essd-14-2129-2022

Cook, D. R. (2016). Towers handbook. In R. Stafford (Ed.), *ARM Climate Research Facility*. DOE/SC-ARM/TR-050. https://doi.org/10.2172/1020277

de Boer, G., Borenstein, S., Calmer, R., Cox, C., Rhodes, M., Choate, C., et al. (2022). Measurements from the University of Colorado RAAVEN uncrewed aircraft system during ATOMIC. *Earth System Science Data*, *14*(1), 19–31. https://doi.org/10.5194/essd-14-19-2022

de Boer, G., Butterworth, B. J., Elston, J. S., Houston, A., Pillar-Little, E., Argrow, B., et al. (2024). Evaluation and intercomparison of small uncrewed aircraft systems used for atmospheric research. *Journal of Atmospheric and Oceanic Technology*, *41*(2), 127–145. https://doi.org/10.1175/JTECH-D-23-0067.1

DeCosmo, J., Katsaros, K. B., Smith, S. D., Anderson, R. J., Oost, W. A., Bumke, K., & Chadwick, H. (1996). Air–sea exchange of water vapor and sensible heat: The Humidity Exchange over the Sea (HEXOS) results. *Journal of Geophysical Research*, *101*(C5), 12001–12016. https://doi.org/10.1029/95jc03796

Donelan, M. A., Drennan, W. M., & Katsaros, K. B. (1997). The air–sea momentum flux in conditions of wind sea and swell. *Journal of Physical Oceanography*, *27*(10), 2087–2099. https://doi.org/10.1175/1520-0485(1997)027<2087:tasmfi>2.0.co;2

Donelan, M. A., Haus, B. K., Reul, N., Plant, W. J., Stiassnie, M., Graber, H. C., et al. (2004). On the limiting aerodynamic roughness of the ocean in very strong winds. *Geophysical Research Letters*, *31*(18), L18306. https://doi.org/10.1029/2004GL019460

Drennan, W. M., Graber, H. C., Hauser, D., & Quentin, C. (2003). On the wave age dependence of wind stress over pure wind seas. *Journal of Geophysical Research*, *108*(C3), 8062. https://doi.org/10.1029/2000JC000715

Drennan, W. M., Kahma, K. K., & Donelan, M. A. (1999). On momentum flux and velocity spectra over waves. *Boundary-Layer Meteorology*, *92*(3), 489–515. https://doi.org/10.1023/a:1002054820455

Drennan, W. M., Zhang, J. A., French, J. R., McCormick, C., & Black, P. G. (2007). Turbulent fluxes in the hurricane boundary layer. Part II: Latent heat flux. *Journal of the Atmospheric Sciences*, *64*(4), 1103–1115. https://doi.org/10.1175/JAS3889.1

Dyer, A. J. (1974). A review of flux-profile relationships. *Boundary-Layer Meteorology*, *7*(3), 363–372. https://doi.org/10.1007/BF00240838

Edson, J. B., Jampana, V., Weller, R. A., Bigorre, S. P., Plueddemann, A. J., Fairall, C. W., et al. (2013). On the exchange of momentum over the open ocean. *Journal of Physical Oceanography*, *43*(8), 1589–1610. https://doi.org/10.1175/JPO-D-12-0173.1

Emanuel, K. A. (1986). An air–sea interaction theory for tropical cyclones. Part I: Steady-state maintenance. *Journal of the Atmospheric Sciences*, *43*(6), 585–605. https://doi.org/10.1175/1520-0469(1986)043<0585:AASITF>2.0.CO;2

Emanuel, K. A. (1995). Sensitivity of tropical cyclones to surface exchange coefficients and a revised steady-state model incorporating eye dynamics. *Journal of the Atmospheric Sciences*, *52*(22), 3969–3976. https://doi.org/10.1175/1520-0469(1995)052<3969:SOTCTS>2.0.CO;2

Foreman, R. J., & Emeis, S. (2010). Revisiting the definition of the drag coefficient in the marine atmospheric boundary layer. *Journal of Physical Oceanography*, *40*(10), 2325–2332. https://doi.org/10.1175/2010JPO4420.1

French, J. R., Drennan, W. M., Zhang, J. A., & Black, P. G. (2007). Turbulent fluxes in the hurricane boundary layer. Part I: Momentum flux. *Journal of the Atmospheric Sciences*, *64*(4), 1089–1102. https://doi.org/10.1175/JAS3887.1

Haus, B. K., Jeong, D., Donelan, M. A., Zhang, J. A., & Savelyev, I. (2010). Relative rates of sea–air heat transfer and frictional drag in very high winds. *Geophysical Research Letters*, *37*(7), L07802. https://doi.org/10.1029/2009GL042206

Hersbach, H. (2011). Sea surface roughness and drag coefficient as functions of neutral wind speed. *Journal of Physical Oceanography*, *41*(1), 247–251. https://doi.org/10.1175/2010JPO4567.1

Hock, T. F., & Franklin, J. L. (1999). The NCAR GPS dropwindsonde. *Bulletin America Meteorology Social*, *80*(3), 407–420. https://doi.org/10.1175/1520-0477(1999)080<0407:TNGD>2.0.CO;2

Högström, U. (1988). Non-dimensional wind and temperature profiles in the atmospheric surface layer: A re-evaluation. *Boundary-Layer Meteorology*, *42*(1–2), 55–78. https://doi.org/10.1007/BF00119875

Högström, U., Smedman, A., Sahleé, E., Drennan, W. M., Kahma, K. K., Pettersson, H., & Zhang, F. (2009). The atmospheric boundary layer during swell: A field study and interpretation of the turbulent kinetic energy budget for high wave ages. *Journal of the Atmospheric Sciences*, *66*(9), 2764–2779. https://doi.org/10.1175/2009JAS2973.1

Holthuijsen, L. H., Powell, M. D., & Pietrzak, J. D. (2012). Wind and waves in extreme hurricanes. *Journal of Geophysical Research*, *117*(C9), C09003. https://doi.org/10.1029/2012JC007983

Jarosz, E., Mitchell, D. A., Wang, D. W., & Teague, W. J. (2007). Bottom-up determination of air–sea momentum exchange under a major tropical cyclone. *Science*, *315*(5819), 1707–1709. https://doi.org/10.1126/science.1136466

Jeong, D., Haus, B. K., & Donelan, M. A. (2012). Enthalpy transfer across the air–water interface in high winds including spray. *Journal of the Atmospheric Sciences*, *69*(9), 2733–2748. https://doi.org/10.1175/JAS-D-11-0260.1

Johnson, H. K., Højstrup, J., Vested, H. J., & Larsen, S. E. (1998). On the dependence of sea surface roughness on wind waves. *Journal of Physical Oceanography*, *28*(9), 1702–1716. https://doi.org/10.1175/1520-0485(1998)028<1702:OTDOSS>2.0.CO;2

Kitaigorodskii, S. A., & Volkov, Y. A. (1965). On the roughness parameter of the sea surface and the calculation of momentum flux in the near-water layer of the atmosphere. *Izvestiya - Atmospheric and Oceanic Physics*, *1*, 973–988.

Kjelgaard, S. O. (1988). Theoretical derivation and calibration technique of a hemispherical-tipped, five-hole probe. In *NASA Technical Memorandum 4047*. Retrieved from https://ntrs.nasa.gov/citations/19890004025

Komori, S., Iwano, K., Takagaki, N., Onishi, R., Kurose, R., Takahashi, K., & Suzuki, N. (2018). Laboratory measurements of heat transfer and drag coefficients at extremely high wind speeds. *Journal of Physical Oceanography*, *48*(4), 959–974. https://doi.org/10.1175/JPO-D-17-0243.1

Large, W. G., & Pond, S. (1981). Open ocean momentum flux measurements in moderate to strong winds. *Journal of Physical Oceanography*, *11*(3), 324–336. https://doi.org/10.1175/1520-0485(1981)011<0324:OOMFMI>2.0.CO;2

Large, W. G., & Pond, S. (1982). Sensible and latent heat flux measurements over the ocean. *Journal of Physical Oceanography*, *12*(5), 464–482. https://doi.org/10.1175/1520-0485(1982)012<0464:SALHFM>2.0.CO;2

Moon, I., Ginis, I., Hara, T., & Thomas, B. (2007). A physics-based parameterization of air–sea momentum flux at high wind speeds and its impact on hurricane intensity predictions. *Monthly Weather Review*, *135*(8), 2869–2878. https://doi.org/10.1175/MWR3432.1

Mueller, J. A., & Veron, F. (2009). A sea state–dependent spume generation function. *Journal of Physical Oceanography*, *39*(9), 2363–2372. https://doi.org/10.1175/2009JPO4113.1

Oost, W., Jacobs, C., & Van Oort, C. (2000). Stability effects on heat and moisture fluxes at sea. *Boundary-Layer Meteorology*, *95*(2), 271–302. https://doi.org/10.1023/A:1002678429212

Paulson, C. A. (1970). The mathematical representation of wind speed and temperature profiles in the unstable atmospheric surface layer. *Journal of Applied Meteorology and Climatology*, *9*(6), 857–861. https://doi.org/10.1175/1520-0450(1970)009<0857:TMROWS>2.0.CO;2

Potter, H., Graber, H. C., Williams, N. J., Collins, C. O., Ramos, R. J., & Drennan, W. M. (2015). In situ measurements of momentum fluxes in typhoons. *Journal of the Atmospheric Sciences*, *72*(1), 104–118. https://doi.org/10.1175/JAS-D-14-0025.1

Powell, M. D., Vickery, P. J., & Reinhold, T. A. (2003). Reduced drag coefficient for high wind speeds in tropical cyclones. *Nature*, *422*(6929), 279–283. https://doi.org/10.1038/nature01481

Reichl, B. G., Hara, T., & Ginis, I. (2014). Sea state dependence of the wind stress over the ocean under hurricane winds. *Journal of Geophysical Research: Oceans*, *119*(1), 30–51. https://doi.org/10.1002/2013JC009289

Richter, D. H., Bohac, R., & Stern, D. P. (2016). An assessment of the flux profile method for determining air–sea momentum and enthalpy fluxes from dropsonde data in tropical cyclones. *Journal of the Atmospheric Sciences*, *73*(7), 2665–2682. https://doi.org/10.1175/JAS-D-15-0331.1

Richter, D. H., & Stern, D. P. (2014). Evidence of spray-mediated air-sea enthalpy flux within tropical cyclones. *Geophysical Research Letters*, *41*(8), 2997–3003. https://doi.org/10.1002/2014GL059746

Smith, S. D., Anderson, R. J., Oost, W. A., Kraan, C., Maat, N., De Cosmo, J., et al. (1992). Sea surface wind stress and drag coefficients: The hexos results. *Boundary-Layer Meteorology*, *60*(1–2), 109–142. https://doi.org/10.1007/BF00122064

Taylor, P. K., & Yelland, M. J. (2001). The dependence of sea surface roughness on the height and steepness of the waves. *Journal of Physical Oceanography*, *31*(2), 572–590. https://doi.org/10.1175/1520-0485(2001)031<0572:TDOSSR>2.0.CO;2

23335084, 2025, 8, Downloaded from https://agupubs.onlinelibrary.wiley.com/doi/10.1029/2025EA004305 by Battelle Memorial Institute, Wiley Online Library on [02/09/2025]. See the Terms and Conditions (https://onlinelibrary.wiley.com/terms-and-conditions) on Wiley Online Library for rules of use; OA articles are governed by the applicable Creative Commons License

Toba, Y., Iida, N., Kawamura, H., Ebuchi, N., & Jones, I. S. F. (1990). Wave dependence of sea-surface wind stress. *Journal of Physical Oceanography*, *20*(5), 705–721. https://doi.org/10.1175/1520-0485(1990)020<0705:WDOSSW>2.0.CO;2

van den Kroonenberg, A., Martin, T., Buschmann, M., Bange, J., & Vörsmann, P. (2008). Measuring the wind vector using the autonomous mini aerial vehicle M2AV. *Journal of Atmospheric and Oceanic Technology*, *25*(11), 1969–1982. https://doi.org/10.1175/2008JTECHA1114.1

Vickers, D., Mahrt, L., & Andreas, E. L. (2013). Estimates of the 10-m neutral sea surface drag coefficient from aircraft eddy-covariance measurements. *Journal of Physical Oceanography*, *43*(2), 301–310. https://doi.org/10.1175/JPO-D-12-0101.1

Volkov, Y. A. (1970). Turbulent flux of momentum and heat in the atmospheric surface layer over a disturbed sea-surface. *Izvestiya - Atmospheric and Oceanic Physics*, *6*, 770–774.

Wadler, J. (2024). Black swift technologies S0 data from 24 March 2023 data collection mission [Dataset]. *Zenodo*. https://doi.org/10.5281/zenodo.11397249

Wildmann, N., Ravi, S., & Bange, J. (2014). Towards higher accuracy and better frequency response with standard multi-hole probes in turbulence measurement with remotely piloted aircraft (RPA). *Atmospheric Measurement Techniques*, *7*(4), 1027–1041. https://doi.org/10.5194/amt-7-1027-2014

Zhang, J. A., Black, P. G., French, J. R., & Drennan, W. M. (2008). First direct measurements of enthalpy flux in the hurricane boundary layer: The CBLAST results. *Geophysical Research Letters*, *35*(14), L14813. https://doi.org/10.1029/2008GL034374

Zhang, J. A., Cione, J. J., Kalina, E. A., Uhlhorn, E. W., Hock, T., & Smith, J. A. (2017). Observations of infrared sea surface temperature and air–sea interaction in hurricane Edouard (2014) using GPS dropsondes. *Journal of Atmospheric and Oceanic Technology*, *34*(6), 1333–1349. https://doi.org/10.1175/JTECH-D-16-0211.1

Zhang, J. A., Marks, F. D., Montgomery, M. T., & Lorsolo, S. (2010). An estimation of turbulent characteristics in the low-level region of intense Hurricanes Allen (1980) and Hugo (1989). *Monthly Weather Review*, *139*, 1447–1462. https://doi.org/10.1175/2010mwr3435.1

Zhao, Z., Chan, P. W., Wu, N., Zhang, J. A., & Hon, K. K. (2020). Aircraft observations of turbulence characteristics in the tropical cyclone boundary layer. *Boundary-Layer Meteorology*, *174*(3), 493–511. https://doi.org/10.1007/s10546-019-00487-8

Zhou, X., Hara, T., Ginis, I., D'Asaro, E., Hsu, J., & Reichl, B. G. (2022). Drag coefficient and its sea state dependence under tropical cyclones. *Journal of Physical Oceanography*, *52*(7), 1447–1470. https://doi.org/10.1175/JPO-D-21-0246.1

Zou, Z., Zhao, D., Liu, B., Zhang, J. A., & Huang, J. (2017). Observation-based parameterization of air-sea fluxes in terms of wind speed and atmospheric stability under low-to-moderate wind conditions. *Journal of Geophysical Research: Oceans*, *122*(5), 4123–4142. https://doi.org/10.1002/2016JC012399

23335084, 2025, 8, Downloaded from https://agupubs.onlinelibrary.wiley.com/doi/10.1029/2025EA004305 by Battelle Memorial Institute, Wiley Online Library on [02/09/2025]. See the Terms and Conditions (https://onlinelibrary.wiley.com/terms-and-conditions) on Wiley Online Library for rules of use; OA articles are governed by the applicable Creative Commons License